Investigations of Adsorbed Organic Molecules in Na–Y Zeolite by Xenon-129 NMR

L. C. de Menorval,† D. Raftery, S.-B. Liu,‡ K. Takegoshi,§ R. Ryoo,‖ and A. Pines*

Materials and Chemical Sciences Division, Lawrence Berkeley Laboratory, 1 Cyclotron Road, and Department of Chemistry, University of California, Berkeley, California 94720 *(Received: December 5, 1988; In Final Form: May 20, 1989)*

The adsorption of *n*-hexane, benzene, and trimethylbenzene in Na–Y zeolite supercages has been investigated by use of xenon-129 NMR. As shown by Fraissard and co-workers, xenon-129 is an excellent probe of its environment in zeolites and is sensitive to the number of adsorbed guest molecules. The xenon-129 chemical shift, when extrapolated to zero effective xenon pressure, is 89.7 ± 0.1 ppm for benzene, 89.0 ± 1.3 ppm for trimethylbenzene, and 107.7 ± 1.2 ppm for *n*-hexane at a concentration of two guest molecules per zeolite supercage compared to 58.9 ± 0.5 ppm for empty Na–Y zeolite supercages. This approach is useful for determining the number of adsorbed molecules inside zeolite supercages and gives information about their arrangement within the supercages.

Introduction

Following Fraissard and co-workers, xenon-129 has been used as a sensitive probe of its chemical environment in nuclear magnetic resonance (NMR) experiments on zeolites.[1-6] Xenon-129, with a spin $^1/_2$ nucleus and 26.4% natural abundance, is useful as a probe because of its chemical inertness, its large polarizability, and its relative ease of detection by NMR.[7] Distortions of the diffuse electron cloud due to collisions with its surroundings can be detected as a change of the chemical shift of the xenon nuclear spin, yielding a chemical shift range of more than 5000 ppm. As a result, the xenon resonance has been shown to be sensitive to the structure of the zeolite, as well as the concentration of the xenon itself. From chemical shift data, void space calculations of various zeolites[3] have been made and the dispersion of metal clusters among the zeolite supercages has been investigated.[4] Xenon NMR has also been used to study the preparation of metal–zeolite catalysts.[5] Through magic angle spinning (MAS) NMR of trapped xenon, Ripmeester has observed different chemical shifts of xenon depending on the cavity structure of mordenites and has determined the various cavity dimensions.[6]

It is of interest to investigate whether xenon can be used to study different species adsorbed in the zeolite structure. Fraissard has studied the effects on the void volume of Na–Y supercages by adsorbed water using xenon-129 NMR.[8] Previous experiments by Lechert and co-workers were concerned with the second moment of the proton NMR spectra for adsorbed benzene molecules in faujasite-type zeolite.[9] Our own group has studied the adsorption of hexamethylbenzene in a Na–Y zeolite by xenon-129 and multiple-quantum spectroscopy.[10] The purpose of the present work is to illustrate the use of xenon-129 NMR to characterize xenon interactions with the zeolite support and to study the adsorption of different guest molecules inside the zeolite structure. We have found that xenon-129 NMR is sensitive to the identity of the adsorbed species, to their concentration, and possibly to the molecular arrangement inside the zeolite supercage.

Experimental Section

Samples were prepared by first heating Na–Y zeolite at 400 °C under vacuum (10^{-6} Torr) overnight to desorb water or other contaminant molecules that might be trapped inside. Guest molecules of various sizes and shapes (*n*-hexane, benzene, and trimethylbenzene) were adsorbed into separate samples of Na–Y zeolite either by addition of some of the liquid organic guest species, in the case of trimethylbenzene, or by distillation in the cases of *n*-hexane and benzene. Samples were then heated typically for 1–3 h above the normal boiling point temperature of the bulk guest species to ensure its distribution throughout the zeolite sample volume. Heat treatment has been shown to play a role in the dispersion of the adsorbed guest in the zeolite.[10] Room temperature xenon adsorption isotherms were measured both before and after the guest molecules were introduced into the zeolite. Helium gas was used to determine the dead volume of the sample.

Xenon-129 spectra were obtained primarily on a Nicolet spectrometer operating at 49.8 MHz. FIDs were acquired following a single 90° pulse at approximately 0.5-s intervals. To ensure adequate signal-to-noise ratios, approximately 2000–4000 scans were accumulated for each spectrum, depending on the xenon pressure. Chemical shift data are relative to a 5.0-atm xenon gas sample[1] (referenced to zero xenon pressure), which is at a lower resonance frequency than that of our samples.

Results

Figure 1 illustrates the basic theme of this work. The xenon-129 NMR absorption signal consists of a single, symmetrical line with

† Present address: Laboratoire de Chimie Organique Physique et Cinétique Chimique Appliquées, UA-418 CNRS, ENSCM, 8 rue Ecole Normale, 34075 Montpelier, Cedex-France.

‡ Present address: Institute of Atomic and Molecular Sciences, Academia Sinica, P.O. Box 23-166, Taipei, Taiwan, ROC.

§ Present address: Foundation of Material Science and Technology of Japan, 3-11-1 Kami-Soshigaya, Setagayaku, Tokyo, Japan.

‖ Present address: Department of Chemistry, Korea Institute of Technology, 400 Kusong-dong, Chung-gu, Taejon-shi, Chung Chong nam-do, Korea.

(1) Ito, T.; Fraissard, J. *J. Chem. Phys.* **1982**, *76*, 5225.

(2) Ito, T.; de Menorval, L. C.; Guerrier, E.; Fraissard, J. P. *Chem. Phys. Lett.* **1984**, *111*, 271. Springuel-Huet, M. A.; Ito, T.; Fraissard, J. P. Adsorption of Xenon: A New Method for Studying the Crystallinity of Zeolites. In *Studies in Surface Science and Catalysis*; Jacobs, P. A., et al., Eds.; Elsevier: Amsterdam, 1984; Vol. 18, pp 13–21. Fraissard, J.; Ito, T.; de Menorval, L. C. Nuclear Magnetic Resonance Study of Xenon Adsorbed on Zeolites and Metal-Zeolites. Application to Catalysis Research. In *Proceedings of the 8th International Congress of Catalysis*; Verlag-Chemie: Weinheim, 1984; Vol. III, pp 25–35.

(3) Demarquey, J.; Fraissard, J. *Chem. Phys. Lett.* **1987**, *136*, 314.

(4) de Menorval, L. C.; Fraissard, J.; Ito, T. *J. Chem. Soc., Faraday Trans. 1* **1982**, *78*, 403. Ito, T.; de Menorval, L. C.; Fraissard, J. *J. Chim. Phys.* **1983**, *80*, 573. de Menorval, L. C.; Fraissard, J.; Ito, T.; Primet, M. *J. Chem. Soc., Faraday Trans. 1* **1985**, *81*, 2855.

(5) Scharpf, E. W.; Crecely, R. W.; Gates, B. C.; Dybowski, C. J. *J. Phys. Chem.* **1986**, *90*, 9. Shoemaker, R.; Apple, T. J. *J. Phys. Chem.* **1987**, *91*, 4024. Chmelka, B. F.; Ryoo, R.; Liu, S.-B.; de Menorval, L. C.; Radke, C. J.; Peterson, E. E.; Pines, A. *J. Am. Chem. Soc.* **1988**, *110*, 4465.

(6) Ripmeester, J. A. *J. Am. Chem. Soc.* **1982**, *104*, 289. Ripmeester, J. A. *J. Magn. Reson.* **1984**, *56*, 247.

(7) Reisse, J. *Nouv. J. Chem.* **1985**, *10*, 665.

(8) Fraissard, J.; Guideon, A. *Zeolites* **1988**, *8*, 376.

(9) Lechert, H.; Basler, W. D.; Wittern, K.-P. Nuclear Relaxation Studies of Aromats in Faujasite Type Zeolite. In *Proceedings of the 7th International Zeolite Conference*; Tokyo, 1986. Lechert, H.; Wittern, K.-P. *Ber. Bunsen-Ges. Phys. Chem.* **1978**, *82*, 1054. Kacirek, H.; Lechert, H.; Schweitzer, W.; Wittern, K.-P. NMR Investigation of Mobility Mechanisms of Benzene Molecules in the Cavities of Faujasite Type Zeolites and Connections with Catalytical and Sorption Properties of these Substances. In *The Properties and Applications of Zeolites*; Townsend, R. P., Ed.; Chemical Society: London (Burlington House: London), 1979; pp 164–173. Lechert, H. *Catal. Rev.-Sci. Eng.* **1976**, *14*, 1.

(10) Liu, S.-B.; Chmelka, B. F.; de Menorval, L. C.; Takegoshi, K.; Ryoo, R.; Trecoske, M.; Pines, A. Manuscript in preparation. Ryoo, R.; Liu, S.-B.; de Menorval, L. C.; Takegoshi, K.; Chmelka, B.; Trecoske, M.; Pines, A. *J. Phys. Chem.* **1987**, *91*, 6575.

0022-3654/90/2094-0027$02.50/0

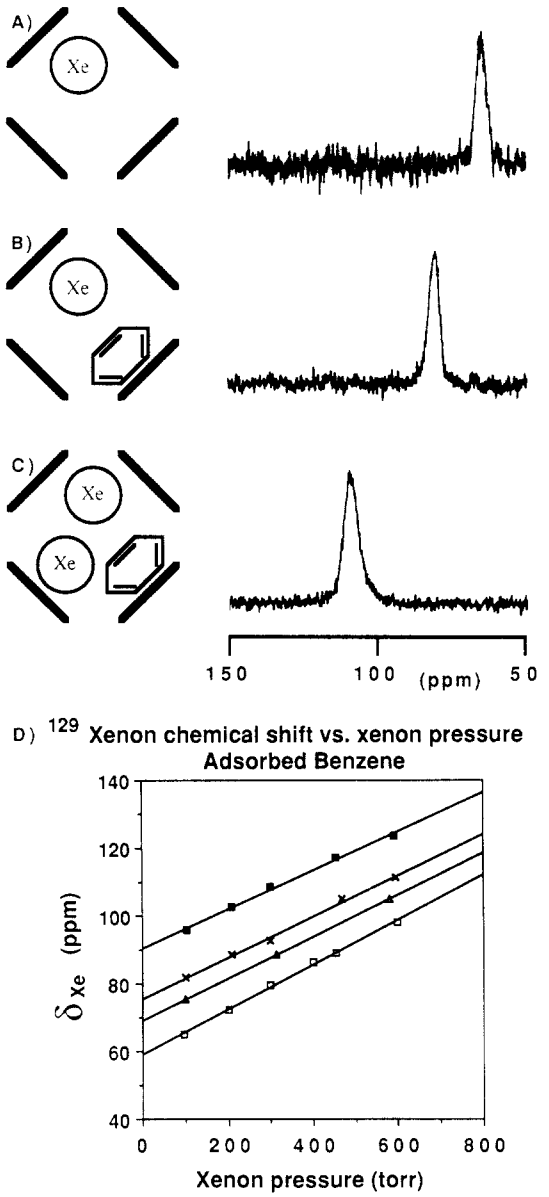

Figure 1. Schematic illustration of a Na–Y supercage with adsorbed (A) xenon (100 Torr), (B) xenon (100 Torr) plus one benzene molecule per cage, and (C) xenon (600 Torr) plus one benzene molecule per cage on the left, and the resulting xenon-129 NMR spectrum for each on the right. (D) shows the full chemical shift data (in units of ppm versus xenon pressure) for adsorbed benzene in concentrations of 0.0 (□), 0.5 (△), 1 (×), and 2 (■) molecules per supercage. T = 21 °C.

a width of approximately 5 ppm. Although the line is partially motionally averaged,[1] the observed line width is probably due to chemical shift anisotropy. The position of the line is a function of both the guest species and its concentration, as well as the density of the xenon inside the supercages of the Na–Y zeolite. The schematic drawing in Figure 1A represents a xenon pressure of 100 Torr, which corresponds (on the average) to one xenon atom per two Na–Y supercages, and the resulting NMR spectrum. The chemical shift is 65.7 ppm at 100 Torr xenon pressure. Adsorption of approximately one benzene molecule per supercage shifts the xenon-129 NMR spectrum downfield to 81.7 ppm as shown in Figure 1B. Increasing the xenon pressure to 600 Torr further increases the chemical shift to 111.5 ppm (Figure 1C).

The full set of chemical shift data for adsorbed benzene in various quantities (0.5, 1, and 2 molecules per supercage) as a function of the equilibrium xenon pressure is shown in Figure 1D. All chemical shift plots are linear functions of the xenon pressure with slopes of approximately 0.060 ppm per Torr of xenon pressure in agreement with previous data on xenon in Na–Y zeolite.[1] The slopes are similar for different amounts of adsorbed benzene, while

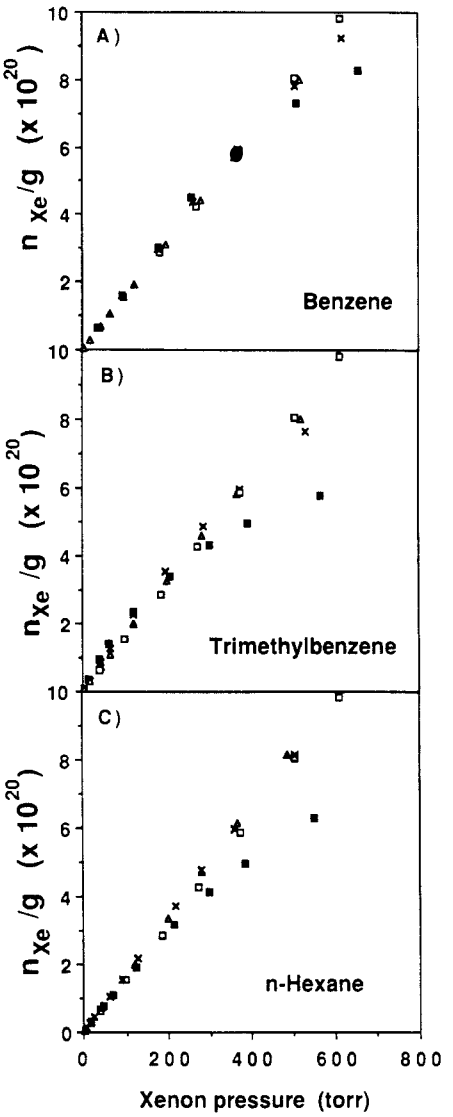

Figure 2. Xenon isotherms at T = 21 °C in empty Na–Y zeolite (□) and with adsorbed guest species in concentrations of 0.5 (△), 1 (×), and 2 (■) guest molecules per supercage. Guest species: (A) benzene, (B) trimethylbenzene, and (C) *n*-hexane.

the chemical shift increases with the concentration of benzene molecules at constant xenon pressure.

Xenon adsorption isotherms in Na–Y zeolite are shown in Figure 2 for various quantities of guest species in the zeolite supercages. The figure displays the effect of guest species loadings corresponding to an average of 0.5, 1, and 2 molecules per zeolite supercage compared with the bare Na–Y zeolite sample. The quantity of xenon adsorbed is plotted against the equilibrium xenon pressure measured at room temperature. The isotherms indicate that adsorption of xenon in the presence of adsorbed guest species is similar in all cases to that of the bare Na–Y support except for xenon pressures above 300 Torr where the effect of the adsorbed molecule becomes significant and the xenon adsorption starts to show some saturation. This feature is most pronounced in Figure 2B for the sample containing (on the average) two trimethylbenzene molecules per zeolite supercage. The xenon adsorption isotherm is significantly different from that of xenon adsorbed in the bare Na–Y sample. Smaller concentrations of trimethylbenzene show less deviation than the case of two molecules per supercage. This deviation is also apparent for the *n*-hexane and benzene samples at high guest molecule concentration, but to a slightly lesser extent than for the trimethylbenzene samples.

To more directly compare the variation of xenon-129 chemical shift versus xenon concentration for the various loadings of guest molecules, data such as those for benzene in Figure 1D can be

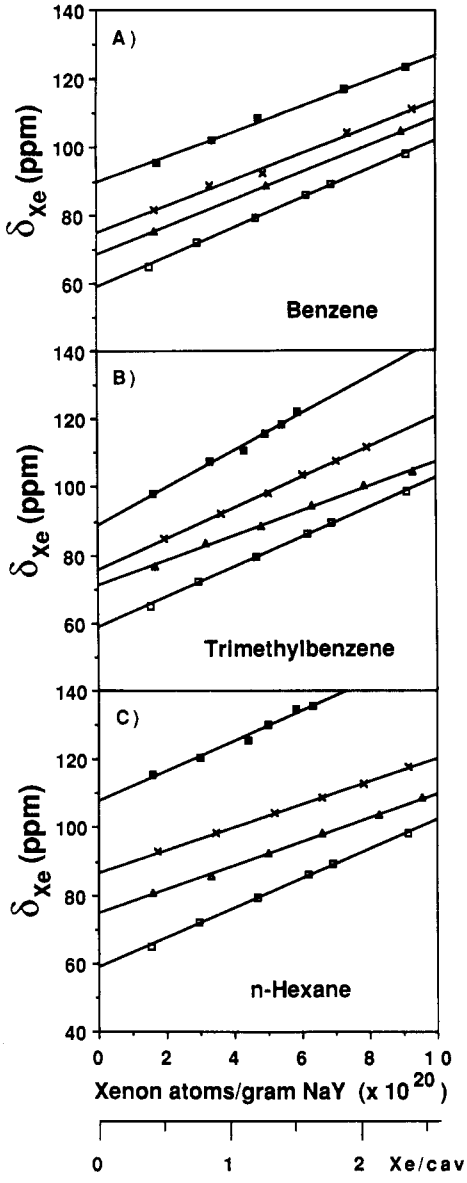

Figure 3. Xenon-129 NMR chemical shift versus xenon concentration (xenon atoms per gram zeolite and atoms per supercage) at $T = 21$ °C for adsorbed guest species in Na–Y zeolite for concentrations corresponding to 0.0 (□), 0.5 (△), 1 (×), and 2 (■) guest molecules per cavity. Guest species: (A) benzene, (B) trimethylbenzene, and (C) *n*-hexane.

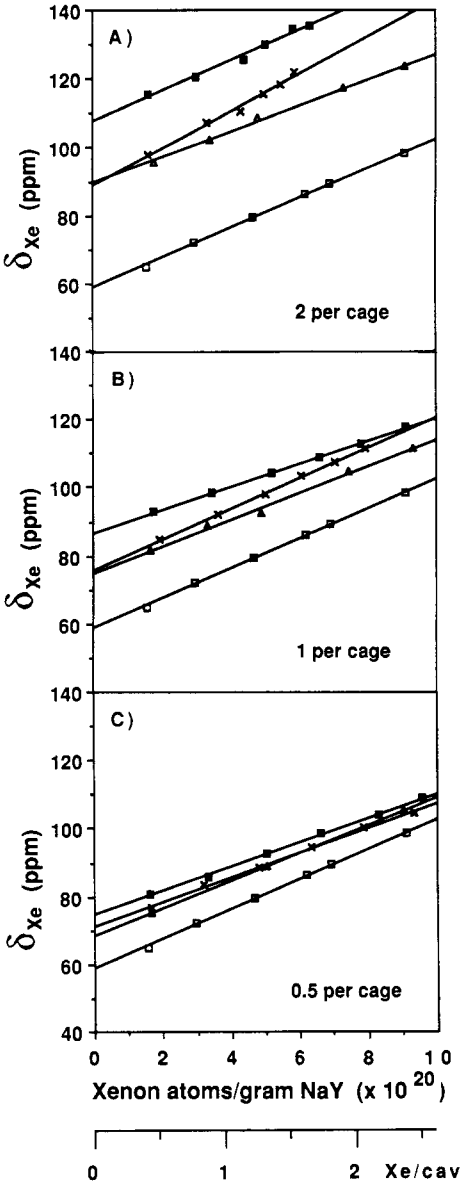

Figure 4. Xenon-129 NMR chemical shift versus xenon concentration (xenon atoms per gram zeolite and atoms per supercage) for adsorbed guest species in Na–Y zeolite: none (□), benzene (△), trimethylbenzene (×), and *n*-hexane (■), for concentrations corresponding to: (A) 2, (B) 1, and (C) 0.5 guest molecules per cavity.

replotted by using the xenon isotherms to convert from xenon equilibrium pressure to xenon concentration (number of xenon atoms adsorbed per gram Na–Y zeolite). Figure 3 shows the chemical shift data for the different guest species at concentrations of 0.5, 1, and 2 molecules per supercage, versus the xenon concentration (as number of xenon atoms per gram of zeolite). The xenon pressure range used in this study (100–600 Torr) corresponds to xenon concentrations of approximately 0.5–3 xenon atoms per supercage. In Figure 4 the data have been replotted by grouping the samples by guest concentration instead of guest species. The *n*-hexane samples show the largest increase in the chemical shift of xenon with respect to the bare Na–Y zeolite sample for all guest molecule concentrations, while the trimethylbenzene and benzene samples have similar but smaller increases over the bare Na–Y case. It is evident that the slope of the lines connecting the chemical shift values depends on the concentration of the guest molecules in the zeolite and that the slopes are different for different guest molecules.

Discussion

Due to the large size of the channels connecting zeolite supercages, xenon is essentially free to move among many supercages during the time period relevant to the NMR experiment.[1,10] This is evidenced by the appearance of a single line in the NMR spectrum of xenon-129, even in the case where there is less than one guest molecule, on the average, per supercage. Such is not the case for heterogeneous distributions of guest molecules because xenon may experience different environments in the sample: the two environments (empty cages versus cages with guest molecules) may be too far apart to be rapidly averaged on the NMR time scale.[10] But for all cases of dispersed distributions, we find the lines of the xenon resonance to be narrow, with no significant broadening at room temperature even due to the cations and paramagnetic impurities which are present in the zeolite lattice.

Jameson and Jameson have shown that the xenon-129 chemical shift can be written as a sum of contributions corresponding to isolated xenon atoms plus collisions between the xenon atoms, the most important of which are two-body collisions.[11] Fraissard and co-workers have extended this idea by adding terms that take into account the interaction of xenon with the zeolite surface, exchangeable cations, metal particles included in the supercages,

(11) Jameson, A. K.; Jameson, C. J.; Gutowsky, H. S. *J. Chem. Phys.* **1970**, *53*, 2310. Jameson, C. J.; Jameson, A. K.; Cohen, S. M. *J. Chem. Phys.* **1973**, *59*, 4540.

TABLE I

guest molecule	concn, molecules/cage	δ_{Xe} at $P_{Xe} = 0$, ppm	slope δ_{Xe} vs Xe concn, ppm/(10^{20} Xe/g of Na-Y)
benzene	2	89.7 ± 0.1	3.8 ± 0.1
	1	75.1 ± 1.1	3.9 ± 0.2
	0.5	68.6 ± 0.1	4.0 ± 0.1
trimethylbenzene	2	89.0 ± 1.3	5.4 ± 0.3
	1	75.9 ± 0.4	4.5 ± 0.1
	0.5	71.2 ± 0.7	3.6 ± 0.1
n-hexane	2	107.7 ± 1.2	4.4 ± 0.3
	1	86.7 ± 0.8	3.4 ± 0.2
	0.5	74.7 ± 0.5	3.5 ± 0.1
none (this work)		58.9 ± 0.5	4.4 ± 0.1
none (ref 1)		58 ± 4	4.6 ± 0.2

or adsorbed water.[8,12] We can similarly add another term to describe the interaction of xenon with organic guest molecules inside the zeolite supercages.

By extrapolating the chemical shift values to zero xenon pressure, the effect of xenon–xenon collisions becomes negligible, leaving the xenon–zeolite surface and the xenon–guest molecule terms. In Table I, values of the xenon-129 chemical shift δ_{Xe} are shown for all samples, extrapolated to zero xenon pressure. For empty Na–Y zeolite, the xenon-129 chemical shift is 58.9 ± 0.5 ppm corresponding to the xenon–zeolite surface contribution to the chemical shift, which is in agreement with previous work by Ito and Fraissard.[1] The benzene and trimethylbenzene samples show similar values of δ_{Xe} at all guest species concentrations. At a concentration of two molecules per supercage, δ_{Xe} is 89.7 ± 0.1 benzene and 89.0 ± 1.3 for trimethylbenzene, which are both much larger than the empty Na–Y case. *n*-Hexane shows the largest value of the chemical shift of xenon in our samples, 107.7 ± 1.2 ppm for approximately two guest molecues per supercage at zero xenon pressure. Small errors in the slope and intercept indicate only that the data are linear. The error of any particular chemical shift value is typically 0.5 ppm.

We can draw some conclusions regarding the location of the guest molecules inside the supercages. As has been suggested by Lechert and co-workers in NMR studies,[9] and by de Mallmann and Barthomeuf[13] from their infrared work, benzene is probably attached to the walls of the supercages near cation sites, although it can rotate freely about its 6-fold axis. Trimethylbenzene, having a geometry similar to benzene, and practically the same chemical shift value at zero xenon pressure in our experiments, is most likely attached in a similar manner to the zeolite supercage walls. *n*-Hexane, on the other hand, has a much larger interaction with xenon. One possible scenario to explain the large xenon chemical shift is that the *n*-hexane molecules may not have a preference to be attached parallel to the surface of the supercage, but protrude into the center of the cage, or may block the channels,[14] allowing for a greater interaction with xenon. This is illustrated in Figure 5A for the case of two molecules per supercage. The orientation of *n*-hexane depicted in this figure would explain the large chemical shift values for *n*-hexane as compared with those of benzene and trimethylbenzene, even though one would expect a saturated hydrocarbon such as *n*-hexane to create less distortion of the xenon electron cloud than benzene with its π-electron cloud. By blocking the channels or extending into the volume of the supercage, *n*-hexane is expected to have a higher probability of interaction than guest molecules attached parallel to the surface of the supercage (Figure 5B–D) and thus produce a larger xenon-129 chemical shift value.

We turn now to the differences in the slopes of the chemical shift values versus xenon concentration. The third column of Table I shows the slopes of the best fits (by least squares) to the data. In previous work, the slopes of the chemical shift plots have been

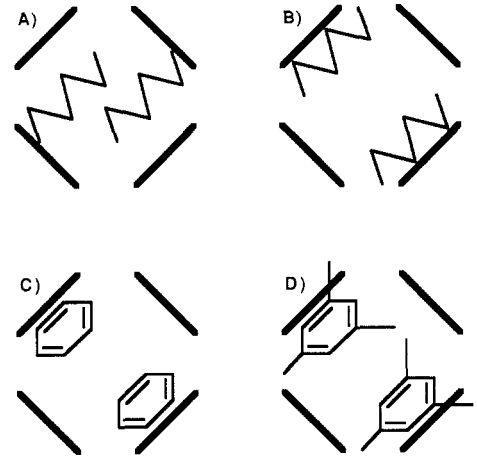

Figure 5. Schematic illustration of the various guest species adsorbed inside the Na–Y zeolite supercages: (A) two *n*-hexane molecules adsorbed normal to the supercage surface, (B) two *n*-hexane molcules adsorbed parallel to the supercage surface, (C) two benzene molecules, and (D) two trimethylbenzene molecules.

related either to the void volume of the supercages[3] or to channel blockage.[12] Blockage of the interconnecting channels would tend to confine the xenon atoms, increasing the xenon atom's collision frequency. Consequently, xenon's chemical shift value would increase due to the increased, time-averaged distortion of the electron cloud. Another factor that could affect the slopes is the size of the guest molecules. High concentrations of large adsorbed guests would decrease the void volume of the supercage, leading again to an increased collision frequency. In this way, both channel blockage and diminished void volume could produce a larger slope in the plot of xenon chemical shift versus adsorbed xenon concentration. Unfortunately, it is not possible to distinguish the effects of these two cases in our present experiments. We can, however, suggest a few explanations that are consistent with our results.

For the three benzene samples, the similarity of the chemical shift slopes indicates that the inclusion of benzene probably does not interfere with xenon by taking up volume in the middle of the supercages or by blocking the channels. This point agrees with previous studies which suggest that benzene is attached to the walls of the supercages.[9,13] The diameter of the zeolite surface near the window (cation site S_{II}) is approximately 6 Å, roughly the kinetic diameter of benzene (see Figure 5C). For the trimethylbenzene case, the situation is not so clear. If trimethylbenzene absorbs like benzene by attaching near the S_{II} cation sites, then it would likely interfere with xenon by blocking the channels due to its larger size. The kinetic diameter of trimethylbenzene is 7.5 Å, so it would extend into the channels as shown in Figure 5D. On the other hand, if trimethylbenzene did not attach to the supercage walls, it could occupy a substantial fraction (up to 40% in the two guest molecule concentration) of the 1100-Å^3 supercage volume. An explanation of the slope data for the *n*-hexane samples is not readily apparent either. One reason for the larger slope seen only at a concentration of two hexane molecules per supercage may be that two hexane molecules are necessary in each supercage to provide an effective net in order to interfere sufficiently with xenon as shown in Figure 5A. Further work is required to resolve these points.

Conclusions

Xenon-129 NMR has been applied to the study of organic molecules adsorbed in Na–Y zeolite, and we find the technique to be sensitive to both the nature and concentration of the adsorbed species. Our results show a difference in the interaction of xenon with aromatic molecules such as benzene and trimethylbenzene as compared to the saturated hydrocarbon chain molecule, *n*-hexane. This difference is probably due to the location of the organic guest inside the Na–Y supercage. We believe that benzene and trimethylbenzene are adsorbed parallel to the zeolite surface

(12) Fraissard, J. NMR Study of ^{129}Xe Adsorbed on Zeolites and Metal-Zeolites. *Z. Phys. Chem. 152*, **1987**, 159–170.
(13) de Mallmann, A.; Barthmeuf, D. Four Different Studies of Benzene Adsorbed in Faujasites. In *Proceedings of the 7th International Zeolite Conference*; Tokyo, 1986 (Elsevier: Oxford), 1986; pp 609–615.
(14) Fraissard, J. private communication.

while *n*-hexane molecules may be adsorbed normal to the surface. We have also found evidence for blocking of the supercage windows due to guest molecule size or orientation.

A complement to this work would be to localize the xenon inside a single supercage either by blocking the channels between the cages or by cooling the sample. Magic angle spinning experiments are under way to compensate for an increase in line width due to the lack of averaging of the anisotropic part of the xenon chemical shift as the temperature is lowered.

Acknowledgment. We thank J. Fraissard and B. F. Chmelka for their comments and suggestions regarding a previous version of this paper. D.R. gratefully acknowledges J. Fraissard for accommodating his stay at the Laboratoire de Chimie des Surfaces in Paris during the spring and summer of 1988, as well as ELF Aquitaine and the Bourse Chateaubriand for financial support. A.P. was a John Simon Guggenheim Fellow. This work was supported by the Director, Office of Energy Research, Office of Basic Energy Sciences, Materials Sciences Division of the U.S. Department of Energy under Contract No. DE-AC03-76SF00098 and by a grant from the Shell Foundation.

Registry No. ^{129}Xe, 13965-99-6; hexane, 110-54-3; benzene, 71-43-2; trimethylbenzene, 25551-13-7.

Consistent Porphyrin Force Field. 1. Normal-Mode Analysis for Nickel Porphine and Nickel Tetraphenylporphine from Resonance Raman and Infrared Spectra and Isotope Shifts

Xiao-Yuan Li,[†] Roman S. Czernuszewicz,[†] James R. Kincaid,[‡] Y. Oliver Su,[†] and Thomas G. Spiro*,[†]

Department of Chemistry, Princeton University, Princeton, New Jersey 08544, and Department of Chemistry, Marquette University, Milwaukee, Wisconsin 53233 (Received: December 20, 1988)

Resonance Raman spectra with variable-wavelength excitation are reported for Ni^{II} porphine (NiP) and for the pyrrole-d_8, meso-d_4, and (pyrrole + meso)-d_{12} isotopomers, as well as for Ni^{II} *meso*-tetraphenylporphine (NiTPP) and its pyrrole-$^{15}N_4$, pyrrole-d_8, $^{13}C_4$-meso, and phenyl-d_{20} isotopomers. All the Raman-active in-plane modes have been identified and are assigned to local coordinates which take into account the phasing of adjacent bond stretches within the pyrrole rings and at the methine bridges. The IR spectra of NiP and its isotopomers are also assigned. For most of the local coordinates good frequency agreement is seen for the different symmetry blocks, showing that longer range phasings have minor effects. These in-plane mode assignments are supported by normal-coordinate calculations with a physically reasonable valence force field, which is nearly the same for NiP and NiTPP. The principal force constants are in good accord with bond length relationships selected on the basis of scaled ab initio calculations. The phenyl substituents of NiTPP lower the frequencies of the asymmetric methine bridge stretching modes $\nu_{10}(B_{1g})$ and $\nu_{19}(A_{2g})$ by $\sim$60 cm^{-1}; this shift is attributable partly to the loss of coupling with the C_mH bending modes in NiP and partly to an electronic effect of the phenyl group. There are also near-resonant interactions in NiTPP between porphyrin and phenyl modes near 740 and 200 cm^{-1} resulting in strongly displaced modes. Otherwise the phenyl groups have little influence on the porphyrin skeletal mode frequencies. Several phenyl modes are subject to moderate RR enhancement, probably via intensity borrowing from nearby porphyrin modes. Large intensities associated with CH bending modes in NiP imply significant excited-state changes in the pyrrole $C_\beta H$ and methine C_mH bond angles. RR spectra for Ni^{II} *meso*-tetramethylporphyrin (TMP) and its methyl-d_{12} isotopomer reveal methyl group modes and somewhat altered skeletal frequencies. Altered polarizations of ν_{10} and ν_{19} in NiTMP and NiTEP (*meso*-tetraethylporphine) reveal a lowering of the effective molecular symmetry, which is attributed to substituent orientation effects. All of these Ni porphyrins show strong overtone and combination band enhancement in resonance with the Q_1 absorption band.

Introduction

Resonance Raman (RR) spectra of metalloporphyrins are of interest[1-13] because of the rich array of spectroscopic phenomena afforded by the electronic properties of the porphyrin chromophore, and also because of the potential for structural characterization in heme proteins. RR spectra of heme proteins have been studied extensively[2] and important regularities have been discovered. It is possible to infer the oxidation, spin, and ligation state of the heme Fe atom with considerable confidence from the frequencies of well-characterized marker bands. No doubt the RR spectra also contain information about more subtle and interesting aspects of heme–protein interactions. Reported spectra of different heme proteins in the same coordination state show numerous differences among bands which have not been well characterized. These differences may be due to protein-imposed distortions of the heme group. It is therefore important to analyze the heme RR vibrational spectrum in as much detail as possible. Ultimately one would like to test structural hypotheses quantitatively with respect to the RR data. Vibrational frequencies for trial structures could be calculated, and compared with experimental data, if a reliable

* Author to whom correspondence should be addressed.
[†] Princeton University.
[‡] Marquette University.

(1) (a) Spiro, T. G.; Li, X.-Y. In *Biological Applications of Raman Spectroscopy*; Spiro, T. G., Ed.; Wiley-Interscience: New York, 1988; Vol. III; Chapter 1. (b) Kitagawa, T.; Ozaki, Y. *Struct. Bonding, Berlin* **1987**, *64*, 71-114.
(2) (a) Spiro, T. G. *Adv. Protein Chem.* **1985**, *37*, 111. (b) Yu, N.-T. *Methods Enzymol.* **1986**, *130*, 350.
(3) (a) Kitagawa, T.; Abe, M.; Ogoshi, H. *J. Chem. Phys.* **1978**, *69*, 4516. (b) Abe, M.; Kitagawa, T.; Kyogoku, Y. *J. Chem. Phys.* **1978**, *69*, 4526.
(4) (a) Choi, S.; Spiro, T. G.; Langry, K. C.; Smith, K. M. *J. Am. Chem. Soc.* **1982**, *104*, 4337. (b) Choi, S.; Spiro, T. G.; Langry, K. C.; Smith, K. M.; Budd, L. D.; La Mar, G. N. *J. Am. Chem. Soc.* **1982**, *103*, 4345. (c) Lee, H.; Kitagawa, T.; Abe, M.; Pandey, R. K.; Leung, H. K.; Smith, K. M. *J. Mol. Struct.* **1986**, *146*, 329.
(5) (a) Willems, D. L.; Bocian, D. F. *J. Am. Chem. Soc.* **1984**, *106*, 880. (b) Willems, D. L.; Bocian, D. F. *J. Phys. Chem.* **1985**, *89*, 234.
(6) Choi, S.; Lee, J. J.; Wei, Y. H.; Spiro, T. G. *J. Am. Chem. Soc.* **1983**, *105*, 3692.
(7) Babcock, G. T. In *Biological Applications of Raman Spectroscopy*; Spiro, T. G., Ed.; Wiley-Interscience: New York, 1988; Vol. III; Chapter 7.
(8) (a) Burke, J. M.; Kincaid, J. R.; Spiro, T. G. *J. Am. Chem. Soc.* **1978**, *100*, 6077 and references therein. (b) Burke, J. M.; Kincaid, J. R.; Peters, S.; Gagne, R. R.; Collman, J. P.; Spiro, T. G. *J. Am. Chem. Soc.* **1978**, *100*, 6083.

0022-3654/90/2094-0031$02.50/0